# JCTC Journal of Chemical Theory and Computation

# Constrained Broyden Minimization Combined with the Dimer Method for Locating Transition State of Complex Reactions

Cheng Shang and Zhi-Pan Liu*

*Shanghai Key Laboratory of Molecular Catalysis and Innovative Materials, Department of Chemistry, MOE Key Laboratory for Computational Physical Sciences, Fudan University, Shanghai 200433, China*

**Abstract:** To determine transition state (TS) and, thus, to predict chemical activity has been a challenging topic in theoretical simulations of chemical reactions. In particular, with the difficulty to compute the second derivative of energy (Hessian) in modern quantum mechanics packages with a non-Gaussian basis set, the location usually involves a high demand in computational power and lacks stability in the algorithm, especially for complex reaction systems with many degrees of freedom. Here, an efficient TS searching method is developed by combining the constrained Broyden minimization algorithm with the dimer method that was first proposed by Henkelman and Jónsson. In the new method, the rotation of the dimer needs only one energy and gradient calculation for determining a rotation angle; the translation of the dimer is continually carried out until a termination criterion is met, and the translational force parallel to the dimer direction is damped to optimize the searching trajectory. Based on our results of the Baker reaction system and of a heterogeneous catalytic reaction, our method is shown to increase the efficiency significantly and is also more stable in finding TSs.

## 1. Introduction

Transition-state theory (TST) plays a central role in chemical kinetics. To determine TS and, thus, to predict chemical activity based on TST is a major theme in modern theoretical simulation of chemical reactions. The algorithms for locating TS can be generally divided into two classes, namely, (i) chain-of-states and (ii) surface-walking methods. The former class simultaneously optimizes a few connected images on the potential energy surface (PES) to identify the minimum energy path (MEP). The representative methods include the nudge elastic band (NEB),[1–5] the doubly nudge elastic band (DNEB),[6–9] and the string methods.[10,11] The later class optimizes only one structural image on the PES by using the local information, such as the gradient (force) or the second derivative (Hessian) of PES. As a result, these methods are much less demanding in computational power. Belonging to this category are the methods, such as the partitioned rational function optimizer (P-RFO),[12–15] the hybrid eigenvector following,[16,17] the dimer,[18–21] and the bond-length constrained minimization methods.[22,23]

Among all the methods in searching for TS, the Hessian involved methods, such as the P-RFO approach, are perhaps the most efficient when the (analytic) Hessian is cheaply available.[15] By modifying and following the eigenvalue of Hessian, these methods can maximize energy in one degree of freedom, while minimizing energy in all the others. To reduce the computational cost in calculating Hessian, the quasi-Newton-based methods have been utilized to update the Hessian, such as the Powell symmetric Broyden (PSB), the symmetric rank 1 (Murtagh–Sargent, MS)[24–28] and the hybrid approach developed by Bofill.[29–34] In practice, a constraint on the step length is often implemented to deal with the overstepping problem.[35] A comprehensive survey for methods in this category has been reviewed by Schlegel.[36]

Different from the P-RFO approach, the dimer method, proposed by Henkelman and Jónsson[18] initially and developed by several other groups[19–21] later, can locate the TS without the need of Hessian. This is particularly advanta-

* Email address: zpliu@fudan.edu.cn.

geous for the cases: (i) when the Hessian is not cheaply available, as in modern quantum mechanics packages with non-Gaussian basis sets and (ii) where a large reaction system with many degrees of freedom is interested.[20,21] The dimer method involves two structural images (defined as a dimer) on the PES, the linkage between which creates a unit vector $\hat{\mathbf{N}}$ separated by a prefixed distance $2\Delta R$ (e.g., $\Delta R = 0.005$ Å). The whole algorithm of the dimer method is constituted by two independent parts, namely rotation and translation. The dimer first rotates to identify the local curvature ($C$), which is equivalent to determine a relevant normal mode of Hessian numerically. The curvature $C$ is calculated using eq 1, where the vectors $\mathbf{F}_2$ and $\mathbf{F}_1$ are the forces acting on each image of the dimer. Then the dimer translates toward the TS. The force for the dimer rotation ($\Delta \mathbf{F}^\perp$) and the translation ($\mathbf{F}_{tran}$) are described by eqs 2 and 3, respectively. In eq 3, $\mathbf{F}_0$ is the total force acting on the middle point of the dimer. The parallel force $\mathbf{F}^\parallel$ ($\mathbf{F}^\parallel \equiv (\mathbf{F}_0 \cdot \hat{\mathbf{N}}) \cdot \hat{\mathbf{N}}$) is defined as the force component parallel to the dimer direction $\hat{\mathbf{N}}$, and the vertical force $\mathbf{F}^\perp$ is defined by $\mathbf{F}^\perp \equiv \mathbf{F}_0 - \mathbf{F}^\parallel$.

$$C = \frac{(\mathbf{F}_1 - \mathbf{F}_2) \cdot \hat{\mathbf{N}}}{2\Delta R} \qquad (1)$$

$$\Delta \mathbf{F}^\perp = (\mathbf{F}_1 - \mathbf{F}_2) - [(\mathbf{F}_1 - \mathbf{F}_2) \cdot \hat{\mathbf{N}}] \cdot \hat{\mathbf{N}} \qquad (2)$$

$$\mathbf{F}_{tran} = \begin{cases} -\mathbf{F}^\parallel = -(\mathbf{F}_0 \cdot \hat{\mathbf{N}}) \cdot \hat{\mathbf{N}} & (C > 0) \\ \mathbf{F}^\perp - \mathbf{F}^\parallel = \mathbf{F}_0 - 2(\mathbf{F}_0 \cdot \hat{\mathbf{N}}) \cdot \hat{\mathbf{N}} & (C < 0) \end{cases} \qquad (3)$$

In the first version of the dimer method, four energy and gradient calculations are required to determine a rotation angle.[18] To reach a converged curvature, the dimer usually needs to rotate 5−10 times, each with a determined rotation angle. The rotation of the dimer is, therefore, the most time demanding part in TS searching. To improve the efficiency, Olsen et al.[19] suggested that the force on the image 2($\mathbf{F}_2$) can be approximated as $\mathbf{F}_2 = 2\mathbf{F}_0 - \mathbf{F}_1$, which can save two energy and gradient calculations in the determination of a rotation angle. Heyden et al. reported a new method to calculate the rotation angle by expanding the rotation angle using the Fourier series.[20] Based on Heyden's approach, Kästner and Sherwood suggested that the rotational force could be extrapolated to save one more energy and gradient calculation, which, however, may hamper the convergence of the rotation.[21] They also reported that by replacing the conjugate gradient (CG) algorithm with the Broyden−Fletcher−Goldfarb−Shanno (L-BFGS) algorithm in the rotation and translation optimizations, the efficiency of the dimer method could be improved.

Recently, we developed a constrained Broyden minimization (CBM) method to locate TS,[23] where the distance of a chemical bond is fixed and autoupdated by the quasi-Newton Broyden method during the TS searching. The method also does not require Hessian as input. Compared to the dimer method, we found that the CBM method eliminates completely the rotation steps as the reaction coordinate is predefined, simply as a bonding pair, and that the CBM carries out the geometry relaxation with multiple Broyden

steps at each fixed bond distance, while the dimer method has only one move (e.g., ≤0.2 Å) at each translation step. These two features make the CBM method efficient in finding simple bond-making/breaking reactions on complex substrates, for example, those often involved in heterogeneous catalysis.[23] However, the CBM method has its own limitation due to the lack of the curvature information; it meets great difficulties in finding complex TS where the reaction coordinate is not so intuitive.

In this work, we aim to develop a better approach by combining the advantages of the dimer and CBM methods to improve the efficiency and the stability in searching for the TS of complex reactions. Indeed, we find that it is possible to integrate the Broyden algorithm in both the rotation and the translation parts of the dimer method. Specifically, our new approach can achieve the following: (i) only one energy and gradient calculation for determining a rotation angle in the dimer rotation; (ii) multiple optimization steps in the dimer translation, similar to the CBM method; and (iii) optimized TS searching trajectory with enhanced stability. By applying to the example reactions, we show that the new algorithm is much more efficient and stable than that of the existing dimer method.

## 2. Methods

Following the terminology of the dimer method, we also describe our algorithm in two sections, namely, the rotation and the translation.

**2.1. Rotation.** The rotation of a dimer can be considered as moving image one ($\mathbf{R}_1$) on a spherical surface, and the center of the sphere is the middle point of the dimer ($\mathbf{R}_0$) with the radius being half of the length of the dimer ($\Delta \mathbf{R}$). The rotation direction was suggested as eq 4, according to Fourier series expansion.[20] To determine the rotation angle $\phi_{min}$, one needs first make a trial rotation of angle $\phi_1$ to obtain the value of $|\Delta \mathbf{F}_{\phi_1}^\perp|$. In total, two energy and gradient calculations ($\Delta \mathbf{F}\perp$ and $\Delta \mathbf{F}_{\phi_1}^\perp$) are thus essential for one rotation (rotate a $\phi_{min}$). Equation 4 may be modified slightly by utilizing the projected $|\Delta \mathbf{F}_{\phi_1}^\perp|$ expressed as $(\Delta \mathbf{F}_{\phi_1}^\perp \cdot \Delta \mathbf{F}^\perp)/|\Delta \mathbf{F}^\perp|$, instead of $|\Delta \mathbf{F}_{\phi_1}^\perp|$.[37] The rotation of the dimer is terminated only if the $\Delta \mathbf{F}\perp$ is below a preset criterion (e.g., rms force ($|\mathbf{F}|$) < 0.05 eV/Å), which typically requires more than five rotations (i.e., ten energy and gradient calculations).

$$\varphi_{min} = \frac{1}{2}\arctan\left(\frac{\sin(2\varphi_1) \cdot |\Delta \mathbf{F}^\perp|}{|\Delta \mathbf{F}^\perp| \cdot \cos(2\varphi_1) - |\Delta \mathbf{F}_{\varphi_1}^\perp|}\right) \qquad (4)$$

We note that by merely minimizing the rotational force $\Delta \mathbf{F}^\perp$ in the rotational step, the determined curvature of the dimer may not necessarily be the lowest eigenvalue (normal mode) of Hessian, since $\Delta \mathbf{F}^\perp$ is diminished at any eigenvalue of Hessian. Heyden et al.,[20] using the P-RFO method with the computed Hessian, showed that the TS searching by always following the lowest curvature could be unstable, i.e., either converge to the wrong TS or fail to converge. Therefore, an algorithm that can most efficiently reduce the rotational force $\Delta \mathbf{F}^\perp$ (i.e., finding the local curvature) is perhaps the most appropriate for the dimer method, provided that a reasonably guessed initial curvature is available.

Following the CBM method, in this work, we utilized the quasi-Newton Broyden method to minimize the rotational force of the dimer. This is addressed in eq 5, where $x$ is chosen as the middle point of the dimer $\mathbf{R}_0$ and $\mathbf{R}_1$, and the residual $R$ is the rotation force $\Delta\mathbf{F}^\perp$. It might be mentioned that the Broyden method has been widely used in electronic structure calculations for both charge density mixing and structural optimization.[23,38] The Broyden method[38–41] iteratively updates its Jacobian ($\mathbf{J}$) matrix (approximate Hessian) or the inverse Jacobian ($G$) based on the iteration history, the equations of which have been derived based on the least-squares minimization of an error function, eq 6. The formula for the modified Broyden method as derived by Johnson[41] is summarized in eqs 7−11. The modified Broyden method has no requirement to store the full (3N × 3N) Hessian matrix.[41,42]

$$x_{i+1} = x_i - \mathbf{J}^{-1}R_i \tag{5}$$

$$E = w_0^2\|G^{(m+1)} - G^{(m)}\| + \sum_{n=1}^{m} w_n^2 \left| \Delta x^{(n)} \rangle + G^{(m+1)} \left| \Delta R^{(n)} \rangle \right|^2 \tag{6}$$

$$G^{(m+1)} = G^{(1)} - \sum_{k=1}^{m} |Z_k^{(m)}\rangle\langle\Delta R^{(k)}| \tag{7}$$

$$|Z_k^{(m)}\rangle = \sum_{n=1}^{m} \beta_{kn}|u^{(n)}\rangle + w_0^2 \sum_{n=1}^{m-1} \beta_{kn}|Z_n^{(m-1)}\rangle \tag{8}$$

$$|u^{(n)}\rangle = G^{(1)}|\Delta R^{(n)}\rangle + |\Delta x^{(n)}\rangle \tag{9}$$

$$\beta_{kn} = (w_0^2 I + a)_{kn}^{-1} \tag{10}$$

$$a_{ij} = w_i w_j |\Delta R^{(j)}\rangle\langle\Delta R^{(i)}| \tag{11}$$

$$\mathbf{R}_1^{new} = \frac{\mathbf{R}_1' - \mathbf{R}_0}{\Delta R'} \times \Delta R \tag{12}$$

It is noted that because $\Delta\mathbf{F}^\perp$ is normal to the dimer $\mathbf{N}$, a direct act of $\Delta\mathbf{F}^\perp$ on the dimer will drive the image $\mathbf{R}_1$ away from the spherical surface of the rotation. To restore the dimer length, we utilize eq 12 to constrain $\mathbf{R}_1$ back to the sphere of rotation along the new dimer direction, where $\mathbf{R}_1'$ and $\mathbf{R}_1^{new}$ are the images before and after the constraint, respectively, and $\Delta R'$ is the length between $\mathbf{R}_1'$ and $\mathbf{R}_0$ ($\Delta R' = |\mathbf{R}_1' - \mathbf{R}_0|$).

**2.2. Translation.** Strictly speaking, the translation direction of the dimer, as guided by the curvature from the rotation, is only meaningful locally, i.e., in a small region defined by $\sim\Delta R$ length on the PES. However, the magnitude of even one translational move has to be very large in practice (e.g., 0.2 Å, 40 times larger than $\Delta R$). This would imply that the traditional framework of the dimer method: one-rotation plus one-translation is not necessarily the safest and the most efficient approach. In principle, it would be desirable to achieve continuous translational moves, i.e., one rotation plus multiple translation, especially with quasi-Newton methods (e.g., BFGS, Broyden) that rely on iteration history to approximate Hessian. With such a framework, the
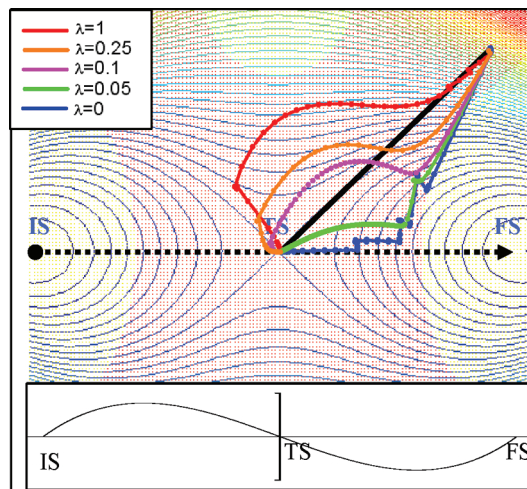


**Figure 1.** TS-searching trajectories on a 2D PES defined by $E = x^4 + 4x^2y^2 - 2x^2 + 2y^2$. The red region is with one negative curvature (mode), and the inflection point locates at the edge of the red region. The insertion at the bottom of the figure shows how $|\mathbf{F}^\parallel|$ varies from the IS to the FS along MEP, as labeled by the dotted arrow. The dotted color curves represent the trajectories with different $\lambda$ values as shown in eq 14.

computational cost may be much reduced, since the rotation of the dimer dominates the computational efforts (in doing energy and gradient calculations). The multiple translation steps with an approximate normal mode can, indeed, be used to locate the TS, as already demonstrated in the CBM method in our recent work,[23] where a bond distance is fixed during geometry relaxation. The key challenge is, therefore, to identify a valid criterion for the termination of multiple translation steps.

*2.2.1. Testing in a Two-Dimensional PES.* To find a suitable criterion, we first investigated a simple two-dimensional (2D) PES defined as $E = x^4 + 4x^2y^2 - 2x^2 + 2y^2$, as shown in Figure 1, where the initial state (IS), the TS, and the final state (FS) are labeled. In the figure, the red region contains one negative mode, and the other areas are all positive-curvature regions. The inflection point is located at the edge of the red region. In the insertion, we show that, going from the IS/FS to the TS along MEP, the parallel force $\mathbf{F}^\parallel$ has always a maximum in absolute value, which occurs at the inflection point. This means that one should minimize the parallel force at the negative-curvature region but maximize the parallel force at the positive-curvature region. Based on this, we have utilized the following criterion for the termination of the translational move:

$$\begin{cases} |\mathbf{F}_i^\parallel| > |\mathbf{F}_{i-1}^\parallel| & (C < 0) \\ |\mathbf{F}_i^\parallel| < |\mathbf{F}_{i-1}^\parallel| & (C > 0) \end{cases} \tag{13}$$

where $\mathbf{F}_i^\parallel$ is the $\mathbf{F}^\parallel$ of the current step and $\mathbf{F}_{i-1}^\parallel$ is the $\mathbf{F}^\parallel$ of the last step. This criterion is designed to prevent the dimer from going down hill to the IS/FS or from trapping around the inflection point and, thus, enable multiple geometry relaxation steps. The idea behind this can be described as follows: When the dimer is between an IS (or FS) and an inflection point where the curvature is positive, the dimer

Transition State of Complex Reactions

*J. Chem. Theory Comput., Vol. 6, No. 4, 2010* **1139**

will translate toward the inflection point to maximize the parallel force. As the dimer passes through the inflection point, the parallel force drops, and the translation is stopped due to eq 13. After the inflection point, the recalculated curvature is negative, and the dimer will translate toward a TS to minimize the parallel force according to eq 13. In the case of systems with multiple inflection points along the reaction coordinate, the algorithm works similarly, as the parallel force has the local maximum or minimum at the inflection points. A translation step will be stopped similarly whenever an inflection point is passed. This will gradually lead the dimer away from the inflection points until the TS is located. To avoid the trapping at the shoulder point in a flat PES, it is essential to ensure the curvature of the located TS to be negative enough.

Furthermore, we found that the TS-searching trajectory (translation trajectory) could also be optimized by modifying the translational force. For illustration purposes, we demonstrated the TS-searching method on the simple PES mentioned above with the following program:

(i) Rotate dimer to identify the local curvature (in fact this can be done analytically in the 2D PES).
(ii) Perform the translational moves with the force according to eq 14, where a factor $\lambda$ (between 0 and 1) on $\mathbf{F}^{\|}$ is introduced. The choice of the value of $\lambda$ in real systems will be discussed in the next subsection. Obviously, when $\lambda$ equals to 1, eq 14 is the same as eq 3 for $C < 0$.

$$\mathbf{F}_{\text{tran}} = \mathbf{F}^{\perp} - \lambda \mathbf{F}^{\|} \qquad (14)$$

(iii) Terminate the translation if the condition of eq 13 is reached or if $|\mathbf{F}^{\perp}| < 10^{-5}$. For the $\lambda = 0$ case, one additional move with the force being $-0.1\mathbf{F}^{\|}$ is carried out.
(iv) Repeat i−iii until $|\mathbf{F}| < 10^{-5}$.
(v) Check the final result by calculating the curvature of the converged state. If the curvature is close to zero, then it implies that the search may converge to a "shoulder state". In such a case, we need to guess a better initial condition and to restart the search.

The effect of $\lambda$ on the TS-searching trajectory can be seen clearly by comparing the dotted color curves in Figure 1. The red curve represents the condition of $\lambda = 1$. The blue one represents a trajectory with $\lambda = 0$. Although both the red and the blue curves can finally converge to the TS, they appear to be two extremes from the optimum searching path, the black line in the figure. If we adjust the value of $\lambda$ in between (0 and 1) in eq 14, we can obtain trajectories between the blue and the red curves, such as the orange ($\lambda = 0.25$), the magenta ($\lambda = 0.1$), and the green ($\lambda = 0.05$). Obviously, the magenta curve is the optimum path among the five curves.

We would like to address further the meaning of $\lambda$ from two aspects. Mathematically, the implementation of $\lambda$ effectively projects out a fraction of the forces at the direction defined by the dimer $\hat{\mathbf{N}}$. By doing this, the minimization of the other degrees of freedom is of higher priority compared to that of the $\hat{\mathbf{N}}$ direction. As shown in the Figure 1 blue curve ($\lambda = 0$), the searching trajectory is toward and along

MEP. From a practical point of view, the identified dimer $\hat{\mathbf{N}}$ direction is local, but the translation along $-\mathbf{F}^{\|}$ ($\lambda = 1$) is typically at a long step size (e.g., 0.2 Å). As a result, the translation with $\lambda = 1$ on a corrugated PES could be unstable, since the walk against the force may lead to the divergence. Therefore, the scaling of $\mathbf{F}^{\|}$ is desirable for safety.

*2.2.2. Implementation in Real Molecular Systems.* In a real system of $3N$ degrees of freedom, eq 14 can be applied similarly for the $C < 0$ regions. The value of $\lambda$ can be conveniently chosen as a set of values, as shown in eq 15, according to the rms value of $\mathbf{F}^{\|}$ ($|\mathbf{F}^{\|}|$) at the beginning of each translation ($\lambda$ is unchanged in one translation). It should be mentioned that by applying $\lambda$ values in between 0 and 1, the TS searching is actually constrained, and the algorithm becomes more stable because the trajectory is closer to MEP. This will be demonstrated in Section 3.

$$\mathbf{F}_{\text{tran}} = \mathbf{F}^{\perp} - \lambda \mathbf{F}^{\|} \quad (C < 0); \quad \lambda =$$

$$\begin{cases} 0.1 & |\mathbf{F}^{\|}| \in [2, +\infty) \\ 0.25 & |\mathbf{F}^{\|}| \in [1, 2) \\ 0.5 & |\mathbf{F}^{\|}| \in [0.5, 1) \\ 1.0 & |\mathbf{F}^{\|}| \in [0, 0.5) \end{cases} \text{(eV/Å)} \quad (15)$$

$$\mathbf{F}_{\text{tran}} = \begin{cases} 0.5 \cdot \mathbf{F}^{\perp} - \mathbf{F}^{\|} & (|\mathbf{F}^{\perp}| < 2) \\ \mathbf{F}^{\perp} - 0.5 \cdot \mathbf{F}^{\|} & (|\mathbf{F}^{\perp}| > 2) \end{cases} \text{(eV/Å)} \quad (C > 0)$$

(16)

$$\begin{cases} |\mathbf{F}_i^{\|}| > |\mathbf{F}_{i-1}^{\|}| & (C < 0) \\ |\mathbf{F}_i^{\|}| < |\mathbf{F}_{i-1}^{\|}| \text{ or } |\mathbf{F}_i^{\perp}| > |\mathbf{F}_{i-1}^{\perp}| & (C > 0) \end{cases} \quad (17)$$

For a similar reason, we also introduce a prefactor 0.5 to the $\mathbf{F}^{\perp}$ or $\mathbf{F}^{\|}$ to optimize the searching trajectory in the $C > 0$ regions, as expressed in eq 16. Equation 16 is designed to reduce the vertical force, preferentially when the force is too large (e.g., $|\mathbf{F}^{\perp}| > 2$ eV/Å), which drags the image toward MEP and to maximize the parallel force when the force is small enough ($|\mathbf{F}^{\perp}| < 2$), which drags the image toward the TS. In our work, the vertical force is always applied in the positive-curvature region (c.f., eq 3) to relax the structure to MEP. Accordingly, a criterion as eq 17 is utilized for the termination of translational move. Equation 17 ensures the minimization of the vertical force together with the maximization of the parallel force during the dimer translation in the $C > 0$ regions.

*2.2.3. Performance of Boyden Algorithm at the Negative-Curvature Region.* While the Broyden technique proved to be applicable for minimization problems when the actual Hessian is positive definite, we here utilized the Broyden technique to locate TS, where the actual or the real Hessian matrix has one negative eigenvalue. To enable the Broyden technique to locate the TS as required, the key is to reverse $\mathbf{F}^{\|}$ as $-\mathbf{F}^{\|}$, which effectively changes the curvature at this degree of freedom to be positive. According to eq 1, where $C = -d\mathbf{F}^{\|}/dx$, it is clear that the sign of the $C$ associated with the parallel force is changed by inverting $\mathbf{F}^{\|}$. Such transformed forces fed into Broyden enables the update of the Jacobian matrix, according to the modified

***Table 1.*** Illustration of the Modified Broyden Algorithm in Finding the Minimum Point (IS) and the Saddle Point (TS) on a Simple Five Dimension PES System[a]

| iteration | $|\bar{\mathbf{x}}|$ | $x_1$ | $x_2$ | $x_3$ | $x_4$ | $x_5$ |
|---|---|---|---|---|---|---|
| IS |  |  |  |  |  |  |
| 0 | 2.8591 | −0.1000 | −0.2000 | −0.3000 | −0.4000 | −0.5000 |
| 1 | 0.7604 | −1.0950 | −1.1801 | −1.2553 | −1.3211 | −1.3776 |
| 2 | 0.3432 | −1.7772 | −1.7473 | −1.7174 | −1.6891 | −1.6635 |
| 3 | 0.0134 | −1.5612 | −1.5641 | −1.5660 | −1.5674 | −1.5683 |
| 4 | 0.0041 | −1.5742 | −1.5727 | −1.5718 | −1.5714 | −1.5711 |
| 5 | 0.0000 | −1.5708 | −1.5708 | −1.5708 | −1.5708 | −1.5708 |
| TS |  |  |  |  |  |  |
| 0 | 2.8591 | −0.1000 | −0.2000 | −0.3000 | −0.4000 | 0.5000 |
| 1 | 0.7604 | −1.0950 | −1.1801 | −1.2553 | −1.3211 | 1.3776 |
| 2 | 0.3432 | −1.7772 | −1.7473 | −1.7174 | −1.6891 | 1.6635 |
| 3 | 0.0134 | −1.5612 | −1.5641 | −1.5660 | −1.5674 | 1.5683 |
| 4 | 0.0041 | −1.5742 | −1.5727 | −1.5718 | −1.5714 | 1.5711 |
| 5 | 0.0000 | −1.5708 | −1.5708 | −1.5708 | −1.5708 | 1.5708 |

[a] The $|\bar{\mathbf{x}}|$ measures the difference of the current position with respect to the converged position.

Broyden algorithm, to be positive definite. In our implementation of the multiple translation steps at $C < 0$ region, once the Jacobian matrix becomes nonpositive definite, which is an indication that the reversed $\mathbf{F}^{\parallel}$ does not fully quench the negative mode, the translation should always be terminated, and a new iteration to rotate the dimer will start. We would like to emphasize that both CG and L-BFGS methods have been utilized in the previous versions of the dimer method,[18–21] which demonstrated that it is, in principle, possible to utilize the minimization techniques to locate the TS with the reversed parallel force.

To illustrate this more clearly, we show the searching for the minimum point and the saddle point with the modified Broyden algorithm on a simple five dimension PES $E = \sum_{i=1}^{5} E_i$, where $E_i = \sin(x_i)$. From Table 1, we can see that when the initial $x_i$ are given as (−0.1,−0.2,−0.3,−0.4,and −0.5), the Broyden can locate the minimum ($-\pi/2, -\pi/2, -\pi/2, -\pi/2,$ and $-\pi/2$), as expected in five steps where $E = -5$. Next, we changed the initial $x_i$ to (−0.1,−0.2,−0.3, −0.4, and 0.5) where the last dimension is close to the maximum (the Hessian has one negative eigenvalue). By reversing the force at this dimension only ($-F_5$) but keeping the right force at the other dimensions, the Broyden can locate both the maximum in this dimension and the minima in the other dimensions, ($-\pi/2, -\pi/2, -\pi/2, -\pi/2,$ and $\pi/2$). The efficiency is the same as the location of the minima, and the Jacobian matrix from Broyden has been verified to be positive definite.

## 3. Results and Discussion

To test the efficiency of our approach, we first chose the Baker reaction system[43] as the testing examples, which contains 25 different chemical reactions as listed in Table 2. The same system has been utilized to test the modified dimer method, according to the reference.[20,21] In this work, four different algorithms, denoted as (**00**), (**01**), (**10**), and (**11**), were implemented to test the individual efficiency of the rotation and translation parts. The algorithms (**00**): the CG dimer method, as reported in refs 20 and 37; (**01**): the same as (**00**) except that the translation uses our Broyden

translation algorithm; (**10**): the same as (**00**) except that the rotation uses the constrained Broyden rotation algorithm; and (**11**): our new method.

For all the reactions studied, we started from the same guess structure ($\mathbf{R}_{GS}$), as suggested by Baker.[43] The initial mode for the dimer was set as $\hat{\mathbf{N}}_{ini} = \mathbf{R}_{GS} - \mathbf{R}_{IS}$, except for reaction 10 (*s*-tetrazine → 2HCN + N$_2$), where $\hat{\mathbf{N}}_{ini} = \mathbf{R}_{FS} - \mathbf{R}_{IS}$ was used. All calculations were performed using the SIESTA package[44] with numerical double-$\zeta$-polarization basis set[45,46] at the density functional theory level, in which the GGA-PBE exchange−correlation functional was utilized.[47] The rotation stops if the $|\Delta\mathbf{F}^{\perp}|$ is lower than 0.1 eV/Å. The translation is terminated by the condition of eq 17. The TS searching is converged if the maximum force on each freedom (max $|\mathbf{F}|$) is below 0.1 eV/Å. All the determined TSs have been checked with the literature structure[43] to ensure that the correct TS is identified. In Table 2, our results on the total calculation steps (the number of energy and gradient calculations) are shown. The "###" sign in the table represents that the corresponding method either produces the wrong TS or diverges after 400 steps.

From Table 2, we found that the average number of steps by using (**00**) method is 91.7 for the 21 reactions with located correct TS, and the method fails in three reactions 10, 11, and 15. In the (**11**) method, the average number of steps is reduced to 35.3, which is about 40% of the (**00**) method (the results of reactions 10, 11, and 15 are not included for comparison between methods here after). Importantly, while the (**00**) method fails in three reactions, all the desired TSs have been located using the (**11**) method. By comparing the four methods, we can see that our algorithms on both the rotation and the translation can help to increase the efficiency. Specifically, the modification to the rotation and the translation only can reduce the step numbers by 23 and 51%, respectively. These will be elaborated further in the following.

**3.1. Efficiency of Rotation.** Table 3 compares the efficiency of the rotation between the (**00**) and (**10**) methods. We can see that the total iteration numbers of the two methods are nearly identical (one iteration contains all energy and gradient calculation steps between two consecutive rotations, including those for both rotation and translation). However, the average energy and gradient calculation steps in each rotation are reduced in the (**10**) method, where the Broyden method is utilized for the dimer rotation. On average, the (**00**) method needs 5.0 energy and gradient calculation steps per rotation, and the (**10**) method needs 3.5 energy and gradient calculations per rotation, which means that the Broyden rotation algorithm can save about 30% computational load. Compared with the extrapolation method proposed by Kästner and Sherwood,[21] that can save about 11% computational load in rotation, the constrained Broyden rotation shows the better performance.

One additional feature of Broyden rotation is that it tends to find a local normal mode by minimizing the rotational force and, thus, is more sensitive to the initial mode provided as the input, which is most naturally determined from the guess initial structure as $\hat{\mathbf{N}}_{ini} = \mathbf{R}_{GS} - \mathbf{R}_{IS}$, or from the final state as $\hat{\mathbf{N}}_{ini} = \mathbf{R}_{FS} - \mathbf{R}_{IS}$ in complex PES reactions. This appears to be advantageous in Baker reactions. By utilizing

Transition State of Complex Reactions

*J. Chem. Theory Comput., Vol. 6, No. 4, 2010* **1141**

**Table 2.** The Energy and Gradient Calculation Steps from Four Different Methods in the TS Location of Baker Reactions[a]

| | system | (00) steps | (10) steps | (10) radio | (01) steps | (01) radio | (11) steps | (11) radio |
|---|---|---|---|---|---|---|---|---|
| 1 | HCN → HNC | 71 | 60 | 85% | 66 | 93% | 32 | 45% |
| 2 | HCCH → CCH$_2$ | 93 | 67 | 72% | 52 | 56% | 40 | 43% |
| 3 | H$_2$CO → H$_2$+CO | 62 | 46 | 74% | 39 | 63% | 31 | 50% |
| 4 | CH$_3$O → CH$_2$OH | 68 | 51 | 75% | 37 | 54% | 29 | 43% |
| 5 | ring-opening cyclopropyl | 88 | 73 | 83% | 41 | 47% | 32 | 36% |
| 6 | bicyclo110 butane TS1 | 96 | 80 | 83% | 36 | 38% | 40 | 42% |
| 7 | bicyclo110 butane TS2 | 144 | 101 | 70% | 56 | 39% | 46 | 32% |
| 8 | β-(formyloxy) ethyl | 88 | 67 | 76% | 24 | 27% | 19 | 22% |
| 9 | parent Diels−Alder | 132 | 122 | 92% | 73 | 55% | 52 | 39% |
| 10 | s-tetrazine → 2HCN + N$_2$ | ### | 101 | − | ### | − | 59 | − |
| 11 | rotational TS in butadiene | ### | 119 | − | 51 | − | 29 | − |
| 12 | H$_3$CCH$_3$ → H$_2$CCH$_2$ + H$_2$ | 77 | 63 | 82% | 41 | 53% | 32 | 42% |
| 13 | H$_3$CCH$_2$F → H$_2$CCH$_2$ + HF | 89 | 64 | 72% | 49 | 55% | 41 | 46% |
| 14 | H$_2$CCHOH → H$_3$CCHO | 141 | 116 | 82% | 104 | 74% | 101 | 72% |
| 15 | HCOCl → HCl + CO | ### | 96 | − | 151 | − | 109 | − |
| 16 | H$_2$O + PO$_3^-$ → H$_2$PO$_4$ | 181 | 84 | 46% | 45 | 25% | 35 | 19% |
| 17 | Claisen rearrangement | 127 | 92 | 72% | 44 | 35% | 37 | 29% |
| 18 | silylene insertion | 70 | 58 | 83% | 29 | 41% | 26 | 37% |
| 19 | HNCCS → HNC + CS | 47 | 36 | 77% | 28 | 60% | 25 | 53% |
| 20 | HCONH$_3^+$ → NH$_4^+$ + CO | 113 | 80 | 71% | 46 | 41% | 35 | 31% |
| 21 | rotational TS in acrolein | 67 | 58 | 87% | 22 | 33% | 17 | 25% |
| 22 | HCONHOH → HCOHNHO | 63 | 46 | 73% | 32 | 51% | 25 | 40% |
| 23 | HNC + H$_2$ → H$_2$CNH | 59 | 50 | 85% | 30 | 51% | 25 | 42% |
| 24 | H$_2$CNH → HCNH$_2$ | 109 | 86 | 79% | 46 | 42% | 40 | 37% |
| 25 | HCNH$_2$ → HCN + H$_2$ | 32 | 27 | 84% | 16 | 50% | 17 | 53% |
| | average | 91.7 | 69.4 | 77% | 43.5 | 49% | 35.3 | 40% |

[a] The ratio is the step number with the method referred divided by that with (00) method. The average values listed do not count the reactions 10, 11, and 15, where the (00) or (01) method fails to locate the TS.

**Table 3.** Comparison Between (00) and (10) Methods for TS Location of Baker Reactions (Numbered from 1 to 25, as in Table 2)[a]

| | method | 1 | 2 | 3 | 4 | 5 | 6 | 7 | 8 | 9 | 10 | 11 | 12 | 13 | 14 | 15 | 16 | 17 | 18 | 19 | 20 | 21 | 22 | 23 | 24 | 25 | av |
|---|---|---|---|---|---|---|---|---|---|---|---|---|---|---|---|---|---|---|---|---|---|---|---|---|---|---|---|
| iter | (00) | 9 | 11 | 8 | 9 | 14 | 18 | 24 | 12 | 19 | ### | ### | 12 | 13 | 20 | ### | 12 | 16 | 13 | 7 | 18 | 13 | 9 | 8 | 17 | 5 | 13.0 |
| | (10) | 8 | 12 | 8 | 9 | 14 | 17 | 24 | 12 | 22 | 21 | 27 | 12 | 11 | 19 | 15 | 13 | 16 | 13 | 7 | 14 | 15 | 8 | 8 | 17 | 5 | 12.9 |
| av. rot | (00) | 6 | 6 | 6 | 6 | 4 | 3 | 4 | 5 | 5 | ### | ### | 4 | 5 | 5 | ### | 13 | 6 | 3 | 4 | 5 | 3 | 5 | 5 | 4 | 4 | 5.0 |
| | (10) | 6 | 4 | 4 | 3 | 3 | 3 | 2 | 4 | 4 | 5 | 2 | 3 | 4 | 4 | 4 | 4 | 4 | 2 | 3 | 4 | 2 | 4 | 4 | 3 | 3 | 3.5 |

[a] Listed are the average rotation steps (av. rot) per iteration and the total iteration number (iter). The average values (av) listed do not count the reactions 10, 11, and 15, where the (00) method fails to locate TS.

**Table 4.** Comparison between (00) and (01) Method for TS location of Baker Reactions (Numbered from 1 to 25, as in Table 2)[a]

| | method | 1 | 2 | 3 | 4 | 5 | 6 | 7 | 8 | 9 | 10 | 11 | 12 | 13 | 14 | 15 | 16 | 17 | 18 | 19 | 20 | 21 | 22 | 23 | 24 | 25 | av |
|---|---|---|---|---|---|---|---|---|---|---|---|---|---|---|---|---|---|---|---|---|---|---|---|---|---|---|---|
| iter | (00) | 9 | 11 | 8 | 9 | 14 | 18 | 24 | 12 | 19 | ### | ### | 12 | 13 | 20 | ### | 12 | 16 | 13 | 7 | 18 | 13 | 9 | 8 | 17 | 5 | 13.0 |
| | (01) | 6 | 4 | 3 | 3 | 2 | 2 | 3 | 1 | 3 | ### | 4 | 3 | 3 | 6 | 11 | 3 | 2 | 1 | 1 | 2 | 1 | 2 | 2 | 3 | 1 | 2.6 |
| trans | (00) | 18 | 22 | 16 | 16 | 28 | 36 | 48 | 24 | 38 | ### | ### | 24 | 26 | 40 | ### | 24 | 32 | 26 | 14 | 36 | 26 | 18 | 16 | 34 | 10 | 26.0 |
| | (01) | 18 | 18 | 13 | 18 | 22 | 18 | 25 | 12 | 31 | ### | 31 | 17 | 21 | 62 | 43 | 15 | 35 | 13 | 12 | 20 | 8 | 12 | 10 | 14 | 6 | 19.1 |
| rot | (00) | 55 | 69 | 46 | 53 | 60 | 62 | 96 | 64 | 88 | ### | ### | 53 | 67 | 103 | ### | 155 | 95 | 44 | 27 | 85 | 37 | 47 | 43 | 75 | 22 | 65.7 |
| | (01) | 48 | 34 | 26 | 19 | 19 | 18 | 31 | 12 | 42 | ### | 20 | 24 | 28 | 42 | 108 | 30 | 9 | 16 | 16 | 26 | 14 | 20 | 20 | 32 | 10 | 24.4 |

[a] Listed are the total iteration number (iter) and the total number of energy and gradient calculations in translation (trans) and in rotation (rot). The average values (av) listed do not count the reactions 10, 11, and 15, where the (00) or (01) method fails to locate the TS.

the constrained Broyden rotation algorithm, the (10) method, we show that all the 25 reactions can converge to the correct TS, while the (00) method fails in three reactions.

**3.2. Efficiency of Translation.** Table 4 compares the efficiency of the translation between the (00) and (01) methods. We see that our translation algorithm can decrease the total iteration number greatly, where the iteration number in (01) is only 20% of that in (00). This is largely because the current translation algorithm carries out multiple translational moves along a better trajectory and can move much longer in distance per iteration compared to that of the (00) method. The higher efficiency in translation, in turn, reduces

effectively the number of rotation needed. As the rotation steps involve heavily the energy and gradient calculations, the reduction in the rotation number can save about 63% computational load, as seen from Table 4. Besides, the translation part can also save 27% computational load, which can be attributed to the application of constrained Broyden algorithm.

In order to see more clearly how the multiple translation works, we have generated a three-dimensional (3D) diagram to trace the searching trajectory, as shown in Figure 2, where the x-axis is along IS−FS vector by setting IS at (0,0,0) and FS at (1,0,0), the y-axis is determined by the TS at $(x_{TS},1,0)$

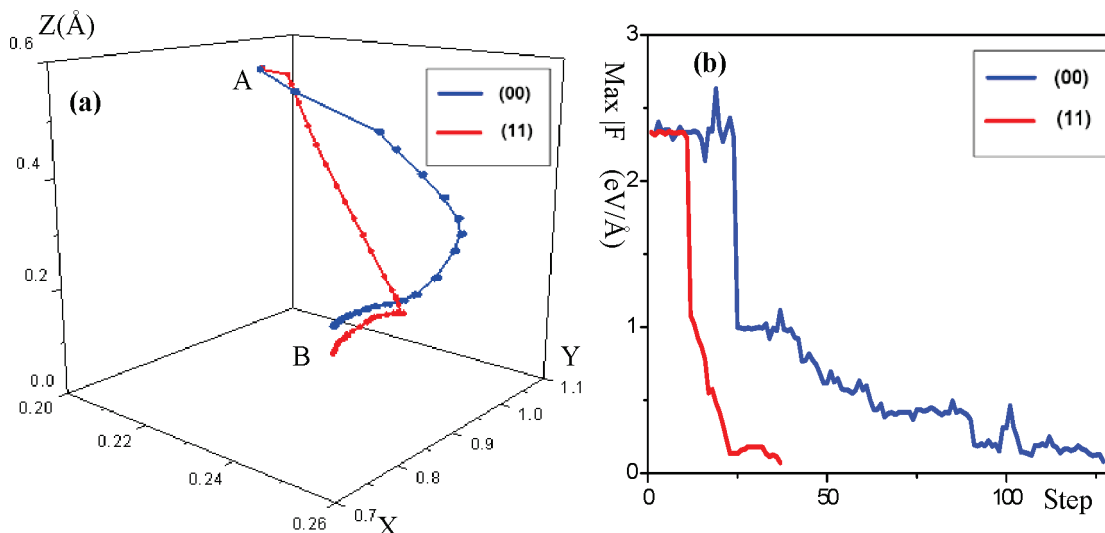**Figure 2.** (a): 3D trajectory of TS searching in Claisen rearrangement reaction. The $x$-axis is along IS−FS vector by setting IS at (0,0,0) and FS at (1,0,0); the $y$-axis is determined by the TS at $(x_{TS},1,0)$ where $x_{TS}$ is the projection of TS on the IS−FS vector; and the $z$-axis is the direction perpendicular to the IS−TS−FS plane. The meaning of the labels are as follows: A is the initial point (guess structure), and B is the end point (located TS). (b): The plot showing the maximum force on each freedom (max $|F|$) in the system during the TS searching.

where $x_{TS}$ is the projection of TS on the IS−FS vector, and the $z$-axis is the direction perpendicular to the IS−TS−FS plane. A large $z$ value of a structure would imply that the structure is far away from the reaction plane (e.g., high in energy) and, thus, is not desirable in TS searching.

Using Claisen rearrangement ($CH_2CHCH_2CH_2CHO \rightarrow CH_2CHOCH_2CHCH_2$) (Figure 2a and b) reaction as the example, we can see two distinct trajectories by using (**00**) and (**11**), as shown by the blue and red curve, respectively. In the 3D figure, the $x$-axis is along IS−FS vector by setting IS at (0,0,0) and FS at (1,0,0); the $y$-axis is determined by the TS at $(x_{TS},1,0)$, where $x_{TS}$ is the projection of TS on the IS−FS vector; and the $z$-axis is the direction perpendicular to the IS−TS−FS plane. The unit vector $\hat{X}$ and $\hat{Y}$ and the $z$ value of an image $R(z_R)$ are defined in eqs 18−20.

$$\hat{X} = \frac{R^{FS} - R^{IS}}{|R^{FS} - R^{IS}|} \quad (18)$$

$$\hat{Y} = \frac{(R^{TS} - R^{IS}) - [(R^{TS} - R^{IS})\bullet\hat{X}]\bullet\hat{X}}{|(R^{TS} - R^{IS}) - [(R^{TS} - R^{IS})\bullet\hat{X}]\bullet\hat{X}|} \quad (19)$$

$$z_R = |(R - R^{IS}) - [(R - R^{IS})\bullet\hat{X}]\bullet\hat{X} - [(R - R^{IS})\bullet\hat{Y}]\bullet\hat{Y}| \quad (20)$$

Peters et al.[48] and Branduardi et al.[49] have suggested methods to measure the distance of a structural image along the reaction coordinate and the displacement from the MEP. These methods need the information of the whole MEP, which is, however, not known practically from the dimer approach. The 3D plot in Figure 2a is, thus, utilized for the comparison of the length of different searching trajectories. Figure 2a shows that there is a turning point in the red curve where the translation of the first iteration meets the termination criterion and where the rotation in the second iteration starts. It appears that the first rotation guides the dimer toward the reaction plane, and the second rotation leads to the exact
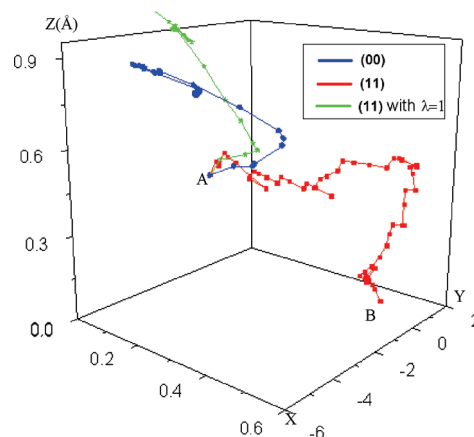


**Figure 3.** 3D trajectory of TS searching in HCOCl → HCl + CO reaction. The meaning of axis and labels are the same as those in Figure 2a.

TS. The red trajectory is shorter than the blue one. The length of the trajectory is 0.99 and 1.40 Å for the red and blue curves, respectively. The red trajectory is close to the straight line distance between A and B ($|R_A - R_B|$), 0.70 Å. With only two rotations and 37 steps, the (**11**) method identifies the TS, whereas there are 16 rotations and 127 steps with the (**00**) method, as compared clearly in Figure 2b, where the maximum force on each freedom in the system is traced during the TS searching. It shows that an efficient translational move can indeed be realized with the approximate mode. The termination criterion for the dimer translation is the key to achieve high efficiency for TS location.

Finally, we would like to address the effect of $\lambda$ in $F_{tran}$ on the TS-searching trajectory. Using the reaction HCOCl → HCl + CO (Figure 3) as the example, we have plotted three trajectories: the blue curve with (**00**) method, the red curve with (**11**) method, and the green curve with (**11**) method but with $\lambda = 1$. Only the red curve finds the TS. In the blue and green curves ($\lambda$ being 1, i.e., by acting $-F^{\parallel}$
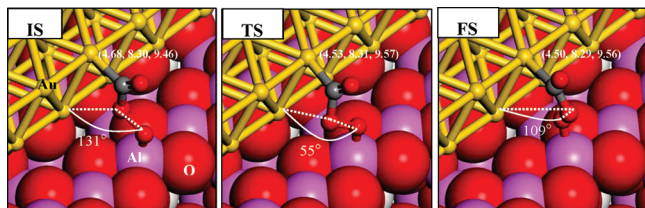
Transition State of Complex Reactions

*J. Chem. Theory Comput., Vol. 6, No. 4, 2010* **1143**



**Figure 4.** Reaction snapshots for a OCOO rotation at the Au/$\gamma$-Al$_2$O$_3$ interface (O, red; Al, purple; H, white; Au, yellow; and C, gray). The Cartesian coordinates of the Au atom that bonds with C is indicated in parentheses.

directly), the structure goes quickly away from the reaction plane due to the too large stretching against the force at the parallel dimer $\hat{\mathbf{N}}$ direction. The trajectory can not be directed back toward the reaction plane because the rotation of the dimer later is localized to the wrong mode. Following such a wrong mode, the TS searching will diverge or lead to undesired TS. Therefore, it can be concluded that with an optimized $\lambda$ factor to $\mathbf{F}^{\|}$, the structure during optimization may leave the unfavorable high-energy region rapidly, and the algorithm is, thus, more stable and efficient.

**3.3. Application in a Large Heterogeneous Catalytic System.** For its no need of the Hessian, the dimer method is well suited for complex reactions occurring in a metallic system, which is not ideal to treat with Gaussian basis sets. Here, we further illustrate our methods in finding a TS involved in the CO oxidation on a Au/$\gamma$-Al$_2$O$_3$ model catalyst, where a two-layer Au strip is deposited on the (100) surface of $\gamma$-Al$_2$O$_3$. The CO oxidation on Au supported on oxides has been studied recently,[50,51] where a bimolecular pathway CO + O$_2$→OCOO occurring at the Au and the oxide interface was identified. The OCOO can further decompose into CO$_2$ and adsorbed O. For the OCOO intermediate at the Au/oxide interface, it has two isomeric structures which are connected by the rotation of OO that is beneath CO. A TS of the rotation can be identified, as shown in the Figure 4, together with the IS and the FS. In the system, 90 degrees of freedom are relaxed, including those of the Au and the top layer $\gamma$-Al$_2$O$_3$ atoms. It should be mentioned that the substrate during the reaction is not rigid with a large displacement from IS to TS, as indicated by the coordinate of the Au atom labeled in Figure 4. The rotation TS is just the kind of TS that is difficult to locate using the CBM method by fixing a certain bond distance.

The above four methods have been applied to locate the TS and the required energy and gradient calculations steps are 511, 353, 197, and 95 for the (**00**), (**10**), (**01**) and (**11**) methods, respectively. We see that, in such a large system, the (**11**) method can also achieve the highest performance, where about 80% CPU time is saved compared to that of the original (**00**) method. The result demonstrates that the dimer rotation and the translation by utilizing the Broyden approach scales well to the large system with many degrees of freedom. For such a large system, the computation of exact Hessian becomes extremely demanding if a numerical algorithm via finite difference method is utilized.

It is noticed that even with the current improvement on efficiency, the average step number of TS location in the Baker system, in this work, is still two times more than that

reported in the original Baker paper, where the P-RFO method (Powell scheme for Hessian update based on an initial analytic Hessian) is utilized. Nevertheless, we would like to emphasize that the dimer method could be the better choice especially when the system is large and when the second derivatives are not available cheaply. This has been addressed previously, as demonstrated by Heyden et al.[20] and Kästner et al.,[21] the original dimer method is already preferable to P-RFO when the Hessian is not cheaply available. We, therefore, believe that the method reported here could be the best choice for locating TSs of large complex reaction systems. Finally, it should be mentioned that compared with the chain-of-states methods, the surface-walking methods, including the dimer method, generally have the so-called "dead-end valley" problem to miss TS off. The dimer method, therefore, also requires a reasonably guessed initial structure in order to locate successfully the desired TS in complex reaction systems. To overcome the problem, Peters et al. has developed a method, which can "teach" saddle search algorithms to locate multiple reaction pathways.[48]

## 4. Conclusion

This work combines the constrained Broyden minimization method with the dimer method for locating TS without the need of Hessian. New algorithms are designed with the aim to maximally cut the rotation steps and to increase the length of translational move. Our method was implemented and tested in the Baker reaction system and also in a large heterogeneous catalytic system, which shows the enhanced stability and the higher efficiency. We demonstrate that the atomic force parallel to the dimer direction can be damped to increase the stability of the TS searching and to shorten the searching trajectory.

## References

(1) Henkelman, G.; Jonsson, H. *J. Chem. Phys.* **2000**, *113*, 9978.

(2) Henkelman, G.; Uberuaga, B. P.; Jonsson, H. *J. Chem. Phys.* **2000**, *113*, 9901.

(3) Mills, G.; Jonsson, H. *Phys. Rev. Lett.* **1994**, *72*, 1124.

(4) Sheppard, D.; Terrell, R.; Henkelman, G. *J. Chem. Phys.* **2008**, *128*, 134106.

(5) Elber, R.; Karplus, M. *Chem. Phys. Lett.* **1987**, *139*, 375.

(6) Trygubenko, S. A.; Wales, D. J. *J. Chem. Phys.* **2004**, *120*, 7820.

(7) Trygubenko, S. A.; Wales, D. J. *J. Chem. Phys.* **2004**, *120*, 2082.

(8) Koslover, E. F.; Wales, D. J. *J. Chem. Phys.* **2007**, *127*, 134102.

(9) Carr, J. M.; Trygubenko, S. A.; Wales, D. J. *J. Chem. Phys.* **2005**, *122*, 234903.

(10) Peters, B.; Heyden, A.; Bell, A. T.; Chakraborty, A. *J. Chem. Phys.* **2004**, *120*, 7877.

(11) E, W. N.; Ren, W. Q.; Vanden-Eijnden, E. *Phys. Rev. B: Condens. Matter Mater. Phys.* **2002**, *66*, 052301.

(12) Simons, J.; Jorgensen, P.; Taylor, H.; Ozment, J. *J. Phys. Chem.* **1983**, *87*, 2745.

(13) Khait, Y. G.; Puzanov, Y. V. *J. Mol. Struct. (THEOCHEM)* **1997**, *398*, 101.

(14) Cerjan, C. J.; Miller, W. H. *J. Chem. Phys.* **1981**, *75*, 2800.

(15) Baker, J. *J. Comput. Chem.* **1986**, *7*, 385.

(16) Munro, L. J.; Wales, D. J. *Phys. Rev. B: Condens. Matter Mater. Phys.* **1999**, *59*, 3969.

(17) Kumeda, Y.; Wales, D. J.; Munro, L. J. *Chem. Phys. Lett.* **2001**, *341*, 185.

(18) Henkelman, G.; Jonsson, H. *J. Chem. Phys.* **1999**, *111*, 7010.

(19) Olsen, R. A.; Kroes, G. J.; Henkelman, G.; Arnaldsson, A.; Jonsson, H. *J. Chem. Phys.* **2004**, *121*, 9776.

(20) Heyden, A.; Bell, A. T.; Keil, F. J. *J. Chem. Phys.* **2005**, *123*, 224101.

(21) Kaestner, J.; Sherwood, P. *J. Chem. Phys.* **2008**, *128*, 014106.

(22) Poppinger, D. *Chem. Phys. Lett.* **1975**, *35*, 550.

(23) Wang, H. F.; Liu, Z. P. *J. Am. Chem. Soc.* **2008**, *130*, 10996.

(24) Powell, M. J. D. *Mathematical Programming* **1971**, *1*, 26.

(25) Schlegel, H. B. *J. Comput. Chem.* **1982**, *3*, 214.

(26) Culot, P.; Dive, G.; Nguyen, V. H.; Ghuysen, J. M. *Theor. Chim. Acta* **1992**, *82*, 189.

(27) Fletcher, R. *Practical Methods of Optimization*, 2nd ed.; Wiley: Chichester, U.K., 1982; Vol. 1.

(28) Dennis, J. E.; Schnabel, R. B. *Numerical Methods for Unconstrained Optimization and Nonlinear Equations*; Prentice-Hall: Englewood Cliffs, NJ, 1983.

(29) Bofill, J. M. *J. Comput. Chem.* **1994**, *15*, 1.

(30) Anglada, J. M.; Besalu, E.; Bofill, J. M.; Rubio, J. *J. Math. Chem.* **1999**, *25*, 85.

(31) Bofill, J. M.; Comajuan, M. *J. Comput. Chem.* **1995**, *16*, 1326.

(32) Bofill, J. M. *Chem. Phys. Lett.* **1996**, *260*, 359.

(33) Anglada, J. M.; Bofill, J. M. *J. Comput. Chem.* **1998**, *19*, 349.

(34) Bofill, J. M.; Anglada, J. M. *Theor. Chem. Acc.* **2001**, *105*, 463.

(35) Besalu, E.; Bofill, J. M. *Theor. Chem. Acc.* **1998**, *100*, 265.

(36) Schlegel, H. B. *J. Comput. Chem.* **2003**, *24*, 1514.

(37) *The FORTRAN code for the cg-dimer method*; Henkelman Research Group: Austin, TX; http://theory.cm.utexas.edu/henkelman. Accessed February 21, 2010.

(38) Kresse, G.; Furthmuller, J. *Comput. Mater. Sci.* **1996**, *6*, 15.

(39) Broyden, C. G. *Mathematics of Computation* **1965**, *19*, 557.

(40) Vanderbilt, D.; Louie, S. G. *Phys. Rev. B: Condens. Matter Mater. Phys.* **1984**, *30*, 6118.

(41) Johnson, D. D. *Phys. Rev. B: Condens. Matter Mater. Phys.* **1988**, *38*, 12807.

(42) Fischer, T. H.; Almlof, J. *J. Phys. Chem.* **1992**, *96*, 9768.

(43) Baker, J.; Chan, F. R. *J. Comput. Chem.* **1996**, *17*, 888.

(44) Soler, J. M.; Artacho, E.; Gale, J. D.; Garcia, A.; Junquera, J.; Ordejon, P.; Sanchez-Portal, D. *J. Phys.: Condens. Matter* **2002**, *14*, 2745.

(45) Junquera, J.; Paz, O.; Sanchez-Portal, D.; Artacho, E. *Phys. Rev. B: Condens. Matter Mater. Phys.* **2001**, *64*, 235111.

(46) Anglada, E.; Soler, J. M.; Junquera, J.; Artacho, E. *Phys. Rev. B: Condens. Matter Mater. Phys.* **2002**, *66*, 205101.

(47) Perdew, J. P.; Burke, K.; Ernzerhof, M. *Phys. Rev. Lett.* **1996**, *77*, 3865.

(48) Peters, B.; Liang, W. Z.; Bell, A. T.; Chakraborty, A. *J. Chem. Phys.* **2003**, *118*, 9533.

(49) Branduardi, D.; Gervasio, F. L.; Parrinello, M. *J. Chem. Phys.* **2007**, *126*, 054103.

(50) Liu, Z. P.; Gong, X. Q.; Kohanoff, J.; Sanchez, C.; Hu, P. *Phys. Rev. Lett.* **2003**, *91*, 266102.

(51) Wang, C. M.; Fan, K. N.; Liu, Z. P. *J. Am. Chem. Soc.* **2007**, *129*, 2642.